High Power Laser Science and Engineering, (2024), Vol. 12, e76, 9 pages.
doi:10.1017/hpl.2024.63

HIGH POWER LASER SCIENCE AND ENGINEERING

RESEARCH ARTICLE

A 1.8 kW high power all-fiber Raman oscillator

Chenchen Fan[1], Xiulu Hao[1], Yang Li[1], Min Fu[1], Zilun Chen[1,2,3], Tianfu Yao[1,2,3], Jinyong Leng[1,2,3], and Pu Zhou[1]

[1]*College of Advanced Interdisciplinary Studies, National University of Defense Technology, Changsha, China*

[2]*Nanhu Laser Laboratory, National University of Defense Technology, Changsha, China*

[3]*Hunan Provincial Key Laboratory of High Energy Laser Technology, Changsha, China*

(Received 14 July 2024; revised 26 August 2024; accepted 11 September 2024)

Abstract

Fiber Bragg grating-based Raman oscillators are capable of achieving targeted frequency conversion and brightness enhancement through the provision of gain via stimulated Raman scattering across a broad gain spectrum. This capability renders them an exemplary solution for the acquisition of high-brightness, specialized-wavelength lasers. Nonetheless, the output power of all-fiber Raman oscillators is typically limited to several hundred watts, primarily due to limitations in injectable pump power and the influence of higher-order Raman effects, which is inadequate for certain application demands. In this study, we introduce an innovative approach by employing a graded-index fiber with a core diameter of up to 150 μm as the Raman gain medium. This strategy not only enhances the injectable pump power but also mitigates higher-order Raman effects. Consequently, we have successfully attained an output power of 1780 W for the all-fiber Raman laser at 1130 nm, representing the highest output power in Raman fiber oscillators with any configuration reported to date.

Keywords: fiber laser; graded-index fiber; Raman oscillator; stimulated Raman scattering

1. Introduction

Raman fiber lasers (RFLs) provide exceptional wavelength flexibility, free from constraints on pump wavelengths, and are capable of operating in cascaded configurations[1–6]. Essentially, they can produce laser wavelengths across the entire fiber transmission window – a feat that is challenging for rare-earth-doped fiber lasers[7–11]. Their compact design, high power scalability and inherent thermal stability make them suitable for high-power applications, sensing and telecommunications[12–14]. Furthermore, they have emerged as a vital tool for generating special wavelength lasers[15–19]. The exploration of stimulated Raman scattering (SRS) within optical fibers for laser emission was initiated as early as the late 20th century and the advent of the 21st century[20–24]. This innovation has illustrated that SRS provides a viable gain mechanism for signal amplification, thereby obviating the necessity for supplementary active elements, including fibers doped with rare-earth elements. With the progression of fiber optic technology, the output power of Raman amplifiers has been markedly enhanced to reach several hundred watts[25–29]. The incorporation of graded-index (GRIN) fibers with increased core diameter, which facilitates the delivery of higher pump power densities into Raman fiber amplifier (RFA) structures, has significantly extended the output power capabilities to the kilowatt range and beyond[4,30,31]. In addition, the intrinsic beam-cleaning properties of GRIN fibers contribute to the maintenance of high-quality output beams, thereby enhancing the overall performance of the RFA systems. However, as power levels escalate, challenges have emerged, including the rapid degradation of beam quality[32], the accelerated growth of second-order Raman light[33] and diminished beam stability[32], limiting further power scaling. While actions such as optimizing the seed beam quality and pump temporal stability can mitigate some of these issues[34], the results have often fallen short of expectations.

Looking forward, achieving signal lasers with higher output power directly within the amplifier structure will likely require the use of GRIN fibers with an enlarged core

Correspondence to: T. Yao and P. Zhou, College of Advanced Interdisciplinary Studies, National University of Defense Technology, Changsha 410073, China. Emails: yaotianfumary@163.com (T. Yao); zhoupu203@163.com (P. Zhou)

diameter. Nonetheless, the advantages of beam cleaning in fibers with an overly large core diameter may not offset the disadvantages introduced by their multimode nature, which could significantly degrade the quality of the laser output beam. In addition, the usage of master oscillator power amplifier (MOPA) structures can augment the output power of laser systems, but also elevates costs and introduces complexities in design and long-term stability. In contrast, oscillator structures offer several advantages, including compactness, stability and cost-effectiveness. The application of advanced grating writing technology can significantly enhance the selection of the fundamental mode within the resonant cavity, thereby improving the laser's beam-cleaning capabilities. The reported researches have also demonstrated that Raman lasers with an oscillator configuration tend to produce superior output beam quality compared to those utilizing an amplifier configuration[35–37]. With the continuous advancement in semiconductor technology and enhancements in the manufacturing of fiber optic components, pump sources with higher power can now be efficiently combined through wavelength division multiplexing (WDM) and optical couplers, and directed into the resonant cavity[25]. This development has enabled the output power of Raman oscillators to reach the hundred-watt range[25]. Nevertheless, the predominant limitation for augmenting power output is still the quantity of pump power that can be introduced, an intrinsic restriction associated with pumping methods that utilize the core of single-mode or few-mode fibers. Employing a cladding pumping method can substantially increase the injectable pump power[29,38], but it presents several challenges. Firstly, the ratio of the cladding area to the core area requires special design to suppress the unwanted higher-order Raman shifts[39]. In addition, the lower brightness residual pump light within the cladding often fails to reach the Raman conversion threshold, leading to excessive residual pump power, diminished Raman conversion efficiency and a larger divergence angle of some of the signal light converted in the cladding. This makes it difficult to filter out the unwanted light, which can severely impact the overall output beam quality of the laser[40,41].The introduction clearly indicates that Raman lasers have now entered the kilowatt era in terms of output power. Nonetheless, the journey towards further advancements is fraught with numerous challenges. For an in-depth exploration of these challenges and the current state of the art, one can refer to the work of Glick *et al.*[42]. Utilizing a multimode GRIN fiber with an enlarged core diameter for core pumping Raman oscillators continues to be the predominant strategy for the realization of high-brightness Raman lasers[43,44]. The current record for output power, achieved through this approach, is 434 W[45]. The critical technical challenge lies in striking a balance between the benefits of increased injectable pump power and enhanced suppression of higher-order Raman effects afforded by a larger core diameter, and the adverse impact on beam-cleaning capability that a larger core diameter can introduce.

In this study, we constructed an all-fiberized Raman oscillator utilizing a specially designed GRIN fiber featuring a 150 μm core diameter. The increased core diameter serves to augment the injectable pump power into the system while concurrently mitigating the impact of higher-order Raman scattering. Utilizing a pump source of elevated brightness, we ensured the beam quality of the laser output. By harnessing the inherent beam-cleaning characteristics of the GRIN fiber, in conjunction with the fundamental mode selection properties of the fiber Bragg grating (FBG), we have successfully attained a high-brightness Raman laser with 1780 W output power, which sets a new record in Raman fiber oscillators across all configurations. In addition, we have undertaken a systematic analysis of the output beam characteristic of power scaling, offering valuable and insightful groundwork for the development of Raman lasers with higher output power and superior beam quality in future endeavors.

2. Experimental setup

The experimental configuration of the Raman fiber oscillator is depicted in Figure 1. The system is pumped by a high-power Yb-doped fiber laser (YDFL), operating at a wavelength of 1080 nm. This laser features an output fiber with a uniform core diameter of 20 μm and a numerical aperture (NA) of 0.06. To augment the pump power and mitigate the impact of backward lasing, which could potentially impair the pump source, a 3×1 tapered fiber bundle (TFB) is utilized for pump injection. The TFB's three input fibers match well with the output fibers of the YDFLs in core diameter, ensuring minimal loss during splicing. The GRIN Raman fiber is specifically engineered with a core/cladding diameter of 150/210 μm and the fiber core features a parabolic refractive index profile with an NA of 0.25, as illustrated in Figure 1(a). The fiber core size was deliberately selected based on detailed considerations. Prior experimental findings have indicated that a GRIN fiber core diameter of up to 100 μm can still produce near-single-mode output due to the beam-cleaning effect induced by SRS[33]. Moreover, an increased fiber size can effectively prevent the signal light from transitioning to the subsequent Stokes light. To enhance the brightness of the pump source, the TFB's output fiber is specifically designed with a core/cladding diameter of 50/400 μm and the NA of the core is 0.12. The length of the GRIN fiber is meticulously optimized to approximately 18 m after evaluating the output power across various lengths. The cavity providing feedback is facilitated by two FBGs with a central wavelength of 1130 nm, which aligns well with the peak of the Raman gain spectrum corresponding to the pump wavelength. The reflection spectra of the FBGs are depicted in Figure 1(b). The high-reflectivity (HR) FBG and output

https://doi.org/10.1017/hpl.2024.63 Published online by Cambridge University Press

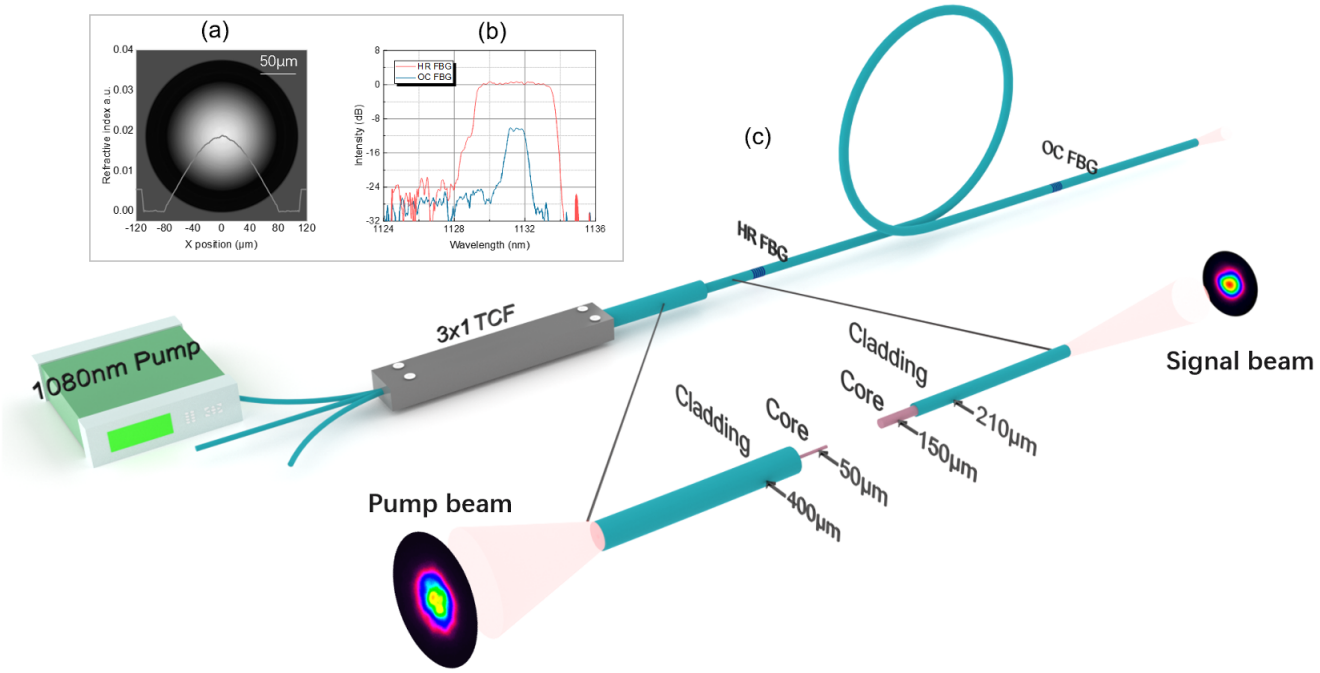

Figure 1. (a) Refractive index profile of the GRIN fiber with 150 μm core diameter. (b) Reflection spectra of the FBGs. (c) Experimental configuration of the GRIN fiber-based Raman fiber oscillator. The right-hand inset depicts the fusion and beam transfer details between the output fiber of the combiner and the GRIN fiber.

coupling (OC) FBG exhibit reflectivities of 99% and 8%, respectively, for low-order transverse modes, with linewidths of approximately 4.5 and 1.1 nm in terms of full width at half maximum (FWHM). It is important to highlight that the reflection of higher-order mode groups, which correspond to the short-wavelength side-lobes in the FBG spectrum, is more than 10 dB lower than that of the fundamental mode. This mode-filtering characteristic of the FBG, attributed to its transverse structure, aids in beam cleanup and contributes to the enhancement of brightness, in conjunction with the Raman gain within the GRIN fiber. Furthermore, an anti-reflection film-coated fiber end cap, designed to cover the spectral range from 1000 to 1200 nm, is spliced to the distal end of the GRIN fiber to reduce end reflection to a minimum. The pump beam, after passing through the TFB, exhibited a speckled intensity distribution, as shown in the left-hand lower inset of Figure 1(c). Despite this, the measured beam quality, characterized by the M^2 factor, remained stable at approximately 7 across various power levels. Following frequency conversion via SRS within the multimode fiber, there was a significant enhancement in the brightness of the signal light. This enhancement is attributed to the higher Raman gain associated with the fundamental mode in the multimode fiber, which facilitates a more efficient energy transfer from higher-order modes to the fundamental mode during the scattering process. Consequently, this results in a more tightly focused beam of the signal laser, as illustrated in the right-hand inset of Figure 1(c).

3. Results and discussion

The output power and spectrum evolution of the RFL as a function of the launched pump power are shown in Figure 2. A dichroic mirror, which has a reflectivity greater than 99% in the range of 1000–1100 nm and a transmissivity greater than 99% from 1100 to 1200 nm, is utilized to separate the output beams at the pump and signal wavelengths for individual measurement. As shown in Figure 2(a), due to the weak Raman gain within the short fiber with a large core, the Stokes light appears at the pump power of 840 W. Beyond this threshold, there is a notable increase in the signal power, which coincides with a rapid decrease in the pump power. Above this threshold, the signal power grows and the pump power simultaneously depletes rapidly. At the maximum pump power of 2494 W, the signal power reaches 1780 W with a residual pump power of 340 W, corresponding to an optical-to-optical conversion efficiency of 71.4%. This result represents the highest reported power for a Raman fiber oscillator in any configuration.

The output spectra of the RFL with filtered pump are presented in Figure 2(b). The 3 dB linewidth of the Stokes signal expands from 0.68 to 1.89 nm when the output power increases from 200 to 1780 W, as a result of the nonlinear effects, such as self-phase modulation and four-wave mixing[32]. In addition, the higher-order Stokes light at 1188 nm emerges when the signal power hits 1200 W. When the signal power rises to 1780 W, the relative peak intensity

https://doi.org/10.1017/hpl.2024.63 Published online by Cambridge University Press

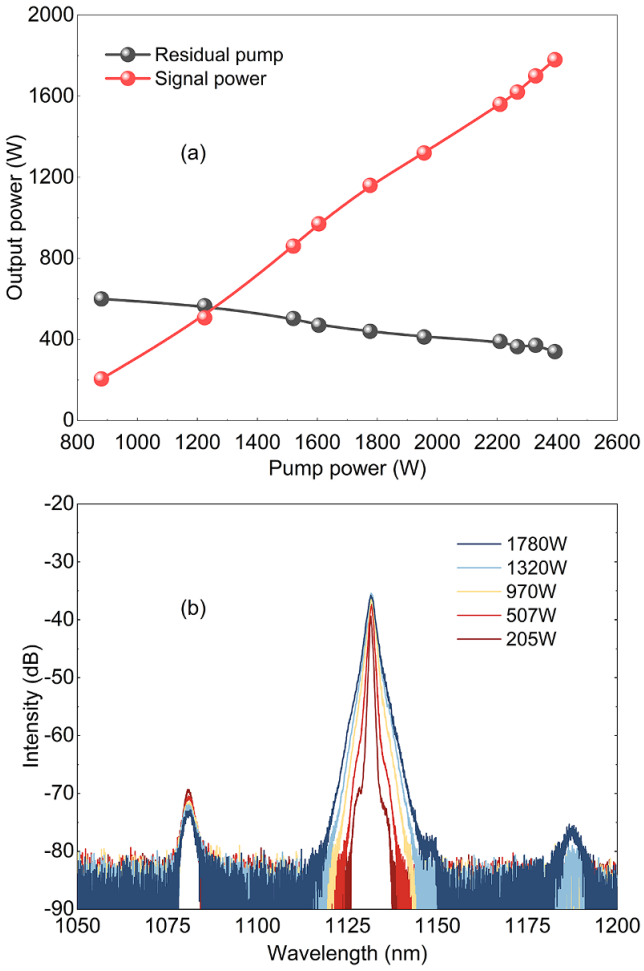

Figure 2. Output power and spectrum evolution of the GRIN fiber-based RFL. (a) Output power evolution of the RFL. With maximum pump power injection of 2494 W, the signal power reaches 1780 W with the undepleted pump power of 340 W, corresponding to an optical-to-optical conversion efficiency of 71.4%. (b) Output spectrum evolution of the RFL. The FWHM linewidth of the Stokes signal broadens from 0.68 to 1.89 nm during power scaling, as a result of the nonlinear effects.

of the light at 1188 nm is approximately 40 dB lower than that of the signal.

To characterize the output performance of the laser system, we measured the near-field output beam profiles at different power levels while systematically assessing their beam quality. The beam quality, as indicated by the M^2 factor, of the RFL was measured at different power levels and is illustrated in Figure 3(b). Considering the potential adverse effects of beam instability at high power levels on measurement accuracy, and to minimize measurement errors, we conducted multiple measurements of the laser beam quality at various power levels. From Figure 3(b), it can be observed that at low power levels, the beam stability is relatively good and the beam quality fluctuation is minimal, with the M^2 value located in the green area. At an output power of 200 W, the average value of M^2 calculated from multiple measurements is 2.5. As the output power increases, the beam quality degrades and the stability of the output beams gradually decreases, manifested as greater fluctuations in the M^2 factor over a wider range. When the output power reaches 1780 W, the average value of the beam quality M^2 factor is 3.5. Utilizing the calculation method for brightness enhancement (BE) detailed by Glick *et al.*[42], we have calculated the BE at various output powers, with the results depicted in Figure 3(b). When the output signal power increased from 205 to 970 W, the corresponding BE factor was enhanced from 1.7 to 2.6, after which it stabilized. At its peak power output, the laser demonstrated a BE factor of 2.6. Although the BE of the laser system did not reach the levels previously reported due to the high pump brightness used in the experiment, it is noteworthy that the system achieved a higher output power within a GRIN fiber-based oscillator structure. The degradation of beam quality can be attributed to the increased power, where Raman conversion leads to mode energy coupling, with more energy flowing from the fundamental mode to higher-order modes.

To verify this hypothesis, we measured the intensity distribution of the near-field beams at different power levels. Also considering the potential impact of beam instability on the measurements, we conducted multiple measurements for each power level. The near-field beam profiles of the RFL at various power levels are monitored by a charge-coupled device (CCD) camera at the focal plane over a period of time, with a sampling frequency of 7.5 Hz and a sampling duration of 10 s. An obvious instability of the output beam can be observed with power scaling. The real-time captured beam profile varies continuously. Figure 3(a) presents one frame image of the beam intensity distribution from the measurement results at different power levels. It can be seen from the figure that at lower power levels, the spot intensity exhibits a bell-shaped distribution with good energy concentration. As the output power increases, more energy that was originally concentrated in the center is transferred to the periphery of the spot, leading to the degradation of beam quality. To systematically understand the modal dynamics characteristics of the Raman conversion process, we constructed a modal decomposition model based on the parallel gradient algorithm[46] to obtain the content of each eigenmode that constitutes its intensity distribution. Considering that the intensity distribution of the output beams retains a bell-shaped distribution, and the maximum beam quality factor M^2 is 3.5, with most of the energy concentrated in the center, our mode decomposition in this case only considers the variation in the content of the first six eigenmodes in the fiber. The row of beam profiles in Figure 3(a) is the reconstructed output beams obtained using these decomposed eigenmodes. The high similarity between the measured (Me) beams and the reconstructed (Re) beams can prove the accuracy of the decomposition algorithm. In addition, we have verified the reliability of the modal decomposition by constructing an evaluation function J,

https://doi.org/10.1017/hpl.2024.63 Published online by Cambridge University Press

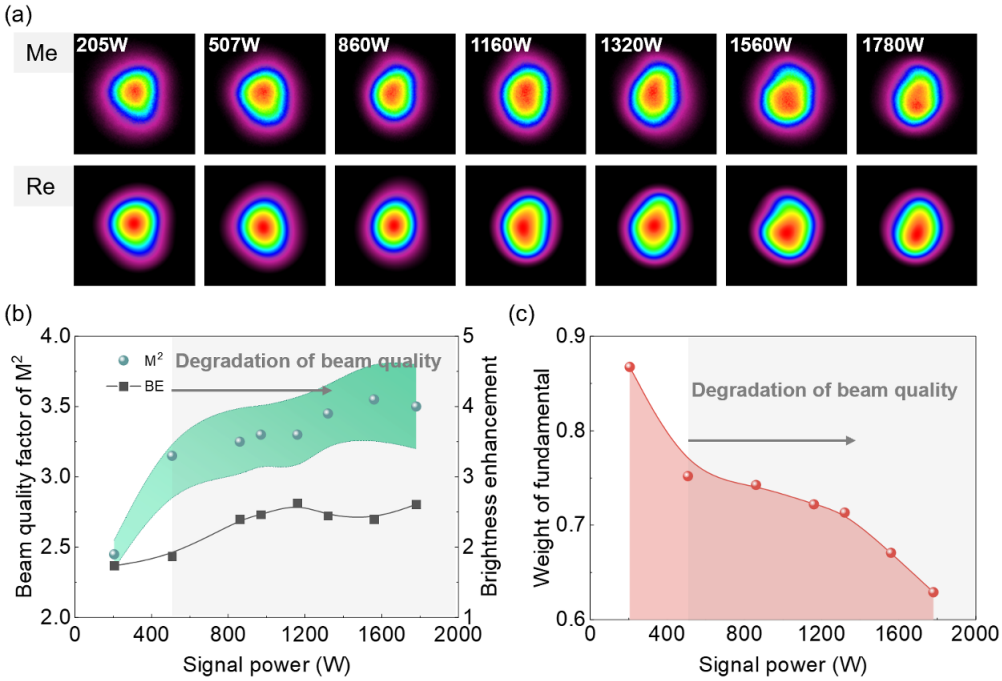

Figure 3. Output beam characteristics of the Raman fiber laser at various powers. (a) The measured and reconstructed beam profiles of the signal laser at various power levels. (b) The M^2 and BE factor of signal light at various power levels. (c) The fundamental mode weight of signal light at various power levels.

whose value ranges from 0 to 1, with values closer to 1 indicating higher accuracy. The J values for the modal decomposition at different power levels all reached above 0.995, which is sufficient to prove the reliability of the decomposition results. After successfully decomposing the output beams at various output powers, we then effectively analyzed the energy coupling between modes during the Raman conversion process. Figure 3(c) shows the variation of the fundamental mode content at various powers, which shows a gradual decline with increasing output power. This process may be due to the thermal effects of quantum losses in the Raman conversion process, which causes nonuniform refractive index modulation of the fiber, leading to the transfer of fundamental mode energy to higher-order modes and a decrease in beam stability.

To evaluate how the stability of the output beams changes with power variations, we employed the mode decomposition algorithm on all these collected beams across various power levels, focusing on the shifts in energy distribution among the beam's internal eigenmodes during the jitter process. The mode decomposition results of 75 speckles collected over a period of 10 s at each power level are shown in Figure 4. The energy among different modes in the beam is constantly coupling over time. Here, we present the variation of the fundamental mode content over time in Figure 4(a). Then, the average value of the measurement results and the standard deviation (Std) are calculated and are shown in Figure 4(b). At a lower power level of 200 W, the average energy occupancy rate of the fundamental mode is 82%. As power increases, the energy coupling process becomes more intense, which is manifested by greater fluctuations in the fundamental mode content, with a larger value of Std. This is the reason for the poor stability of the detected output beams. The average values of the fundamental mode content decrease with power scaling, indicating that more energy is transferred to higher-order modes, leading to a degradation in the measured beam quality. When the output power reaches 1780 W, the average energy occupancy rate of the fundamental mode in the speckle drops to 68%, corresponding to the degraded M^2 value of 3.5.

To provide a more in-depth analysis of the beam instability phenomenon within our laser system, we have examined the temporal dynamics of the output beam. Utilizing a photodiode (PD) detector and an oscilloscope, characterized with a maximum detection bandwidth of 1 GHz and a sampling time interval of 40 μs, we conducted measurements over a 4 s sampling period. The resultant temporal dynamics of the laser output across various power levels are illustrated in Figures 4(c) and 4(d). It can be found that the temporal performance of the RFL is stable with relatively low noise when the output power is lower than 200 W. The normalized Std and coefficient of variation (CV) were calculated and are depicted in Figure 4(d). These metrics exhibit a significant increase with the escalation of power to higher levels, indicating the enhanced intensity fluctuation characteristic of the signal laser. Upon reaching a signal power of 500 W, a discernible reduction in the stability of the output beam is observed, corroborated by an increase

https://doi.org/10.1017/hpl.2024.63 Published online by Cambridge University Press

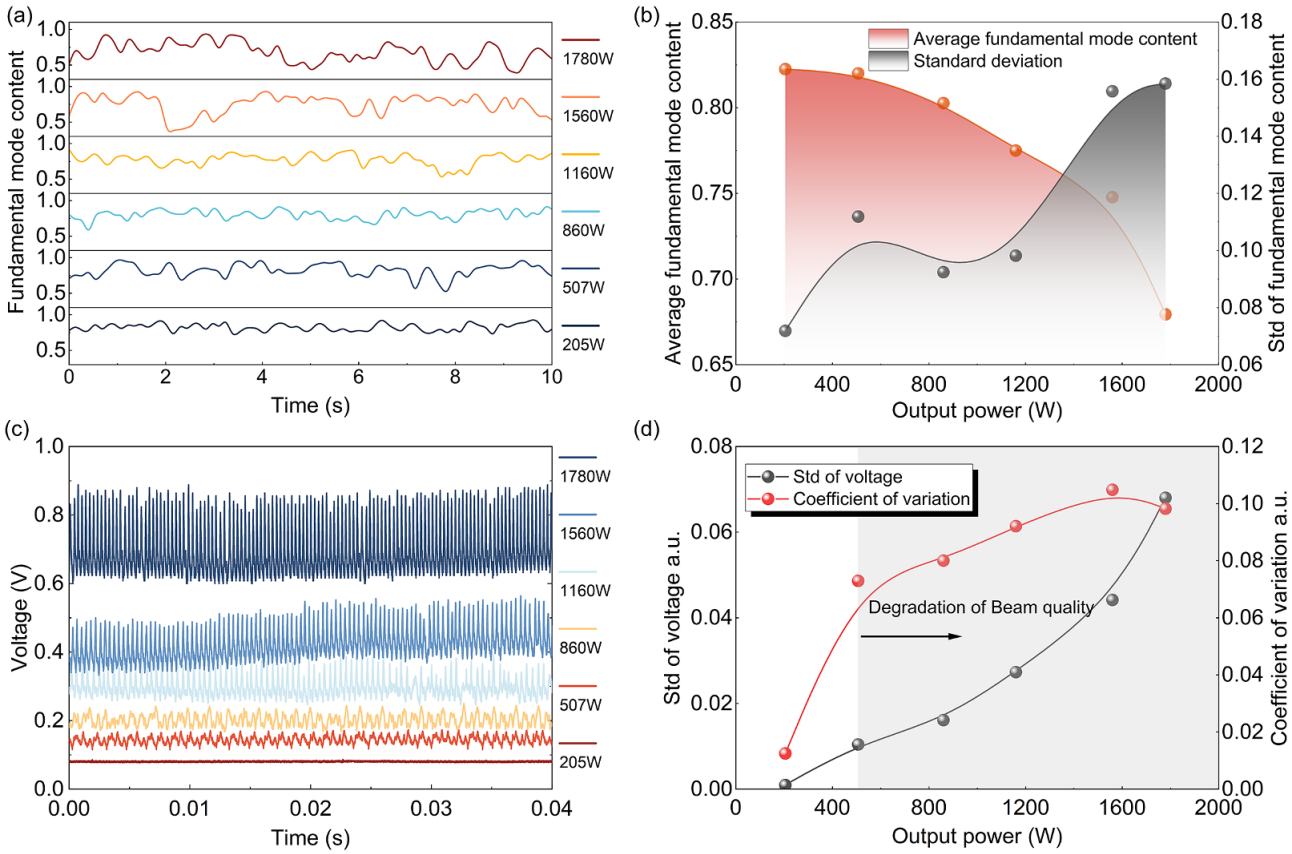

Figure 4. Mode characteristics and temporal dynamics under different output power levels. (a) Temporal variation in the content of the fundamental mode under various power levels. (b) Mean value of the fundamental mode content. (c) Time-domain signal of beam intensity. (d) Standard deviation and coefficient of variation.

in Std and CV values. As the signal light power escalates from 200 to 500 W, the Std of the intensity signal fluctuation rises from 0.1 to 0.5, suggesting a concomitant rise in higher-order mode content and intensified mode coupling within the system. This observation is in line with the trend depicted in Figure 4(b), where a marked decline in fundamental mode content is noted once the power threshold of 500 W is surpassed, and the mode coupling intensity, as indicated by the Std, exhibits a pronounced enhancement. The surge in higher-order mode content and the concomitant reduction in mode stability are also implicated in the degradation of beam quality, as illustrated in Figure 3. Specifically, as the signal light power augments from 200 to 500 W, the beam quality, quantified by the M^2 factor, deteriorates from 2.5 to 3.2.

Similarly, with the mode instability in the YDFL, this phenomenon in the multimode RFL is observed once a certain average power threshold is exceeded and manifests itself in a strong and dynamic energy transfer with beam shape fluctuation. In our experiment, the length of the optical fiber used was only 18 m, and the fiber was well secured and coiled in specially designed grooves on a water-cooled board for cooling. Therefore, the possibility of mode instability caused by fiber disturbance can be ruled out. In our previous studies, it was found that mode instability in Raman lasers is also related to higher-order Raman light[33]. When higher-order Raman light is generated and grows rapidly, the output beam will exhibit increasing mode instability. In this experiment, the content of higher-order Raman light was at a very low level, and this mode instability phenomenon even existed and was observed before the emergence of higher-order Raman light. What can be determined in our experiment is that the increase in the content of higher-order modes and the degradation of beam quality occur simultaneously with mode instability, approximately at a power level of 500 W, and have the same trend of change. Since both the Raman gain in the optical fiber and the feedback of the FBG are mode dependent, the beam with different mode contents inside the fiber will also change its output mode contents after stimulated Raman amplification. Therefore, the cause of the beam instability at the output is the rapid coupling of higher-order modes and the fundamental mode inside the fiber over time. The reason for this rapid coupling is likely to be similar to the cause in the YDFL, where the thermal load caused by quantum loss forms a weak longitudinal periodic modulation of the fiber refractive index, causing periodic mode coupling between the fundamental mode

https://doi.org/10.1017/hpl.2024.63 Published online by Cambridge University Press

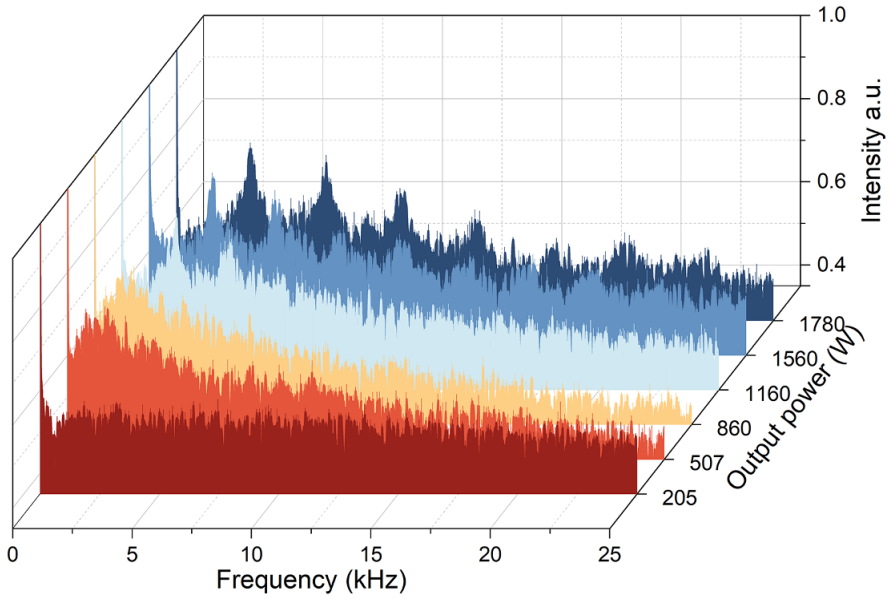

Figure 5. Fourier spectrum of the signal light's temporal intensity at different power levels.

and higher-order modes inside the fiber[47]. In fiber lasers, once the average output power surpasses a certain threshold, transverse mode instability (TMI) often arises, causing a decline in beam quality and a loss of mode stability. A key feature of this process is the energy transfer between the fundamental mode and higher-order modes at a specific frequency, detectable as a fixed characteristic frequency in the Fourier spectrum of the intensity information. This phenomenon is generally attributed to thermal effects, particularly the thermally induced refractive index grating (RIG) within the optical fiber. When the output power exceeds the TMI threshold, phase-matched energy transfer between different transverse modes is necessary. The RIG facilitates this exchange, possessing a periodic internal refractive index distribution that mirrors the modal interference pattern created by the transverse modes. Upon coupling into a fiber with an enlarged core, energy is shared between the fundamental and higher-order modes, leading to a quasi-periodic optical field distribution within the core. This distribution, in turn, affects the thermal profile, resulting in the formation of a RIG through the thermo-optic effect.

To conduct further research and exploration into the phenomenon of modal instability, we performed a Fourier transform on the time-domain intensity signal of the output beam in Figure 4(c), and the results are shown in Figure 5. In our Raman laser system, the fiber with an exceptionally large core diameter supports a multitude of intrinsic modes. As output power increases, the interference pattern between the activated higher-order and lower-order modes induces periodic modulation of the fiber's refractive index. This enables the transfer of optical energy among higher-order, fundamental and lower-order modes at discrete frequencies. The observed multiple characteristic frequencies in spectral analysis are ascribed to the variation in RIGs caused by interference among different modes. When the output power is less than 205 W, the performance of the output beam is relatively stable, and there is no obvious mode dynamic coupling process at this time and no characteristic peaks are observed in the Fourier spectrum. As the output power increases to 507 W, the output beam undergoes slight jitter and a characteristic peak is observed at 2 kHz in the Fourier spectrum, which is mainly the energy coupling between the fundamental mode and low-order modes. As the power further increases to 1160 W, an additional characteristic peak is observed at 5 kHz in the Fourier spectrum, which is due to the mode coupling between the fundamental mode and higher-order modes. As the power further increases, the beam jitter becomes more severe, the characteristic peaks become more pronounced and higher frequency characteristic peaks appear, which is due to the dynamic energy coupling between the fundamental mode and higher-order modes, as well as among higher-order modes themselves. According to the experimental results, it can be observed that using a large-core GRIN fiber can effectively suppress higher-order Raman scattering, enabling higher-power Raman laser output. However, the large-core fiber introduces more higher-order modes, which lowers the threshold for mode instability in the laser system, and speckle jitter is observed at lower power levels. How to further optimize the refractive index parameters and core diameter of the fiber to comprehensively consider the suppression effect of higher-order Raman scattering and the threshold of mode instability will be a key issue to be studied in the future to achieve a higher-power Raman laser output.

https://doi.org/10.1017/hpl.2024.63 Published online by Cambridge University Press

4. Conclusion

In summary, we have constructed an all-fiber Raman oscillator based on a specially designed GRIN fiber. Thanks to the large core diameter and extremely short fiber length, the injectable pump power was effectively enhanced while significantly suppressing higher-order Raman scattering. Under the pump of high-power lasers, a Raman laser output of 1780 W was ultimately achieved, setting the record for the maximum output power of a Raman oscillator reported to date. The combination of a high-brightness pump source and the inherent beam purification of the GRIN fiber effectively enhanced the brightness of the signal light. With the support of grating pairs that have the effect of filtering higher-order modes, the brightness of the output signal light was further enhanced. At the highest power, the beam quality M^2 improved from 7 of the pump light to 3.5 of the signal light. In addition, the laser system exhibited beam jitter and mode instability during the power enhancement process. By systematically measuring and analyzing the output characteristics of the laser, including intensity distribution, mode content and temporal information, the intrinsic connection among mode instability, beam quality degradation and changes in higher-order mode content was clarified. This provides guidance for achieving higher-power RFL output in the next steps.

Acknowledgement

This work was supported by the National Natural Science Foundation of China (Nos. 12174445 and 62061136013).

References

1. S. A. Babin, High Power Laser Sci. Eng. **7**, e15 (2019).
2. V. Balaswamy, S. Aparanji, S. Arun, S. Ramachandran, and V. R. Supradeepa, Opt. Lett. **44**, 279 (2019).
3. W. Chen, M. Hu, Z. Xu, A. Ge, Y. Gao, J. Fan, H. Song, B. Liu, J. Li, and C. Wang, J. Lightwave Technol. **36**, 5237 (2018).
4. Y. Chen, T. Yao, H. Xiao, J. Leng, and P. Zhou, High Power Laser Sci. Eng. **8**, e33 (2020).
5. S. Dong, B. Han, H. Wu, K. Deng, Y. Liu, and Y. Rao, Opt. Laser Technol. **161**, 109094 (2023).
6. W. Pan, L. Zhang, H. Jiang, X. Yang, S. Cui, and Y. Feng, Laser Photonics Rev. **12**, 1700326 (2018).
7. P. Zheng, D. Wu, and S. Dai, Opt. Laser Technol. **164**, 109496 (2023).
8. H. Wu, Z. Wang, W. Sun, Q. He, Z. Wei, and Y.-J. Rao, J. Lightwave Technol. **36**, 844 (2018).
9. M. Bernier, V. Fortin, M. El-Amraoui, Y. Messaddeq, and R. Vallée, Opt. Lett. **39**, 2052 (2014).
10. S. A. Babin, E. A. Zlobina, and S. I. Kablukov, IEEE J. Sel. Top. Quantum Electron. **24**, 1400310 (2018).
11. L. R. Taylor, Y. Feng, and D. B. Calia, Opt. Express **18**, 8540 (2010).
12. C. W. Freudiger, W. Yang, G. R. Holtom, N. Peyghambarian, X. S. Xie, and K. Q. Kieu, Nat. Photonics **8**, 153 (2014).
13. B. H. Hokr, J. N. Bixler, M. T. Cone, J. D. Mason, H. T. Beier, G. D. Noojin, G. I. Petrov, L. A. Golovan, R. J. Thomas, B. A. Rockwell, and V. V. Yakovlev, Nat. Commun. **5**, 4356 (2014).
14. J. Li and M. Zhang, Light Sci. Appl. **11**, 128 (2022).
15. S. Loranger, A. Tehranchi, H. Winful, and R. Kashyap, Optica **5**, 295 (2018).
16. X. Ma, J. Xu, J. Ye, Y. Zhang, L. Huang, T. Yao, J. Leng, Z. Pan, and P. Zhou, High Power Laser Sci. Eng. **10**, e8 (2022).
17. F. Monet, J.-S. Boisvert, and R. Kashyap, Sci. Rep. **11**, 13182 (2021).
18. D. A. Orringer, B. Pandian, Y. S. Niknafs, T. C. Hollon, J. Boyle, S. Lewis, M. Garrard, S. L. Hervey-Jumper, H. J. L. Garton, C. O. Maher, J. A. Heth, O. Sagher, D. A. Wilkinson, M. Snuderl, S. Venneti, S. H. Ramkissoon, K. A. McFadden, A. Fisher-Hubbard, A. P. Lieberman, T. D. Johnson, X. S. Xie, J. K. Trautman, C. W. Freudiger, and S. Camelo-Piragua, Nat. Biomed. Eng. **1**, 0027 (2017).
19. J. Zhou, W. Pan, W. Qi, X. Cao, Z. Cheng, and Y. Feng, PhotoniX **3**, 18 (2022).
20. J. Nilsson, J. K. Sahu, J. N. Jang, R. Selvas, D. C. Hanna, and A. B. Grudinin, in *Optical Amplifiers and Their Applications* (OSA, 2002), paper PD2.
21. C. A. Codemard, P. Dupriez, Y. Jeong, J. K. Sahu, M. Ibsen, and J. Nilsson, Opt. Lett. **31**, 2290 (2006).
22. M. E. Lines, J. Appl. Phys. **62**, 4363 (1987).
23. C. Lin, L. G. Cohen, R. H. Stolen, G. W. Tasker, and W. G. French, Opt. Commun. **20**, 426 (1977).
24. E. Dianov and A. Prokhorov, IEEE J. Sel. Top. Quantum Electron. **6**, 1022 (2000).
25. Y. Feng, L. R. Taylor, and D. B. Calia, Opt. Express **17**, 23678 (2009.
26. C. A. Codemard, J. Ji, J. K. Sahu, and J. Nilsson, Proc. SPIE **7580**, 75801N (2010).
27. M. Rekas, O. Schmidt, H. Zimer, T. Schreiber, R. Eberhardt, and A. Tünnermann, Appl. Phys. B **107**, 711 (2012).
28. V. R. Supradeepa and J. W. Nicholson, Opt. Lett. **38**, 2538 (2013).
29. Y. Shamir, Y. Glick, M. Aviel, A. Attias, and S. Pearl, Opt. Lett. **43**, 711 (2018).
30. Y. Chen, J. Leng, H. Xiao, T. Yao, and P. Zhou, IEEE Access **7**, 28 (2019).
31. Y. Chen, T. Yao, H. Xiao, J. Leng, and P. Zhou, J. Lightwave Technol. **39**, 1785 (2021).
32. Y. Chen, T. Yao, L. Huang, H. Xiao, J. Leng, and P. Zhou, Opt. Express **28**, 3495 (2020).
33. C. Fan, H. Xiao, T. Yao, J. Xu, Y. Chen, J. Leng, and P. Zhou, Opt. Lett. **46**, 3432 (2021).
34. C. Fan, J. Wu, T. Yao, H. Xiao, J. Xu, J. Leng, P. Zhou, A. A. Wolf, I. N. Nemov, A. G. Kuznetsov, and S. A. Babin, Opt. Laser Technol. **172**, 110507 (2024).
35. S. H. Baek and W. B. Roh, Opt. Lett. **29**, 153 (2004).
36. S. I. Kablukov, E. A. Zlobina, M. I. Skvortsov, I. N. Nemov, A. A. Wolf, A. V. Dostovalov, and S. A. Babin, Quantum Electron. **46**, 1106 (2016).
37. E. A. Zlobina, S. I. Kablukov, A. A. Wolf, A. V. Dostovalov, and S. A. Babin, Opt. Lett. **42**, 9 (2017).
38. Y. Glick, Y. Shamir, M. Aviel, Y. Sintov, S. Goldring, N. Shafir, and S. Pearl, Opt. Lett. **43**, 4755 (2018).
39. J. Ji, C. A. Codemard, M. Ibsen, J. K. Sahu, and J. Nilsson, IEEE J. Sel. Top. Quantum Electron. **15**, 129 (2009).
40. Y. Chen, T. Yao, H. Xiao, J. Leng, and P. Zhou, Opt. Lett. **45**, 2367 (2020).
41. C. Fan, Y. An, Y. Li, X. Hao, T. Yao, H. Xiao, L. Huang, J. Xu, J. Leng, and P. Zhou, J. Lightwave Technol. **40**, 6486 (2022).

https://doi.org/10.1017/hpl.2024.63 Published online by Cambridge University Press

42. Y. Glick, Y. Shamir, Y. Sintov, S. Goldring, and S. Pearl, Opt. Fiber Technol. **52**, 101955 (2019).
43. Y. Glick, V. Fromzel, J. Zhang, N. Ter-Gabrielyan, and M. Dubinskii, Appl. Opt. **55**, B97 (2016).
44. E. A. Zlobina, S. I. Kablukov, A. A. Wolf, I. N. Nemov, A. V. Dostovalov, V. A. Tyrtyshnyy, D. V. Myasnikov, and S. A. Babin, Opt. Express **25**, 12581 (2017).
45. C. Fan, Y. Chen, T. Yao, H. Xiao, J. Xu, J. Leng, P. Zhou, A. A. Wolf, I. N. Nemov, A. G. Kuznetsov, S. I. Kablukov, and S. A. Babin, Opt. Express **29**, 19441 (2021).
46. H. Lü, P. Zhou, X. Wang, and Z. Jiang, Appl. Opt. **52**, 2905 (2013).
47. C. Jauregui, C. Stihler, and J. Limpert, Adv. Opt. Photonics **12**, 429 (2020).

https://doi.org/10.1017/hpl.2024.63 Published online by Cambridge University Press